Exploration of the electron multiple recollision dynamics in intense laser fields with Bohmian trajectories

Hossein Z. Jooya,[1],[*] Dmitry A. Telnov,[2] and Shih-I Chu[1],[3],[†]

[1]*Department of Chemistry, University of Kansas, Lawrence, Kansas 66045, USA*
[2]*Department of Physics, St. Petersburg State University, St. Petersburg 199034, Russia*
[3]*Center for Quantum Science and Engineering, Department of Physics, National Taiwan University, Taipei 10617, Taiwan*

Electron multiple recollision dynamics under intense midinfrared laser fields is studied by means of the de Broglie–Bohm framework of Bohmian mechanics. Bohmian trajectories contain all the information embedded in the time-dependent wave function. This makes the method suitable to investigate the coherent dynamic processes for which the phase information is crucial. In this study, the appearance of the subpeaks in the high-harmonic-generation time-frequency profiles and the asymmetric fine structures in the above-threshold ionization spectrum are analyzed by the comprehensive and intuitive picture provided by Bohmian mechanics. The time evolution of the individual electron trajectories is closely studied to address some of the major structural features of the photoelectron angular distributions.

I. INTRODUCTION

Photoelectron rescattering and multiple rescattering processes are in the center of most of the nonlinear phenomena, such as high-order-harmonic generation (HHG) [1,2] and above-threshold ionization (ATI) [3]. A prominent feature of a rescattering (as well as multiple rescattering) process is the interference between the repetitive wave packets initiated within a particular laser cycle and the ones generated at different optical cycles [4]. This does not necessarily imply that the electron revisits the parent ion more than once. The multiple revisits can, however, happen under intense midinfrared laser field. Under these circumstances a small percentage of the ionized wave packets can revisit the parent ion multiple times [5].

The inclusion of the electron-core Coulomb interaction appears to be inevitable in both HHG and ATI theoretical investigations. Each harmonic, in the HHG process, is associated with both short and long trajectories that have the same return energy but different return times [6]. The exploration of the underlying mechanism responsible for essential features of harmonic generation such as cutoff expansion and multiple plateau generation requires accurate quantum mechanical treatment [7]. Detailed analysis of energy features of the strong field ionization has been also the focus of many studies [8–11]. Yan *et al.* [11] presented a semiclassical approach based on quantum orbits to provide a physically intuitive interpretation analysis of the low-energy structures (LESs). Liu *et al.* [10] have shown that the LESs arise due to an interplay between multiple forward scattering of an ionized electron and the electron momentum disturbance by the Coulomb field immediately after the ionization. Hickstein *et al.* [12] used a simple model to associate the shape of these structures with the number of times the ionized electron is driven past its parent ion in the laser field before strongly scattering away. Consequently, multiple rescattering has been

essentially reported to be responsible for the appearance of some of the primary features of the above-threshold ionization (ATI) spectra [10–14]. At the same time, many reports have been dedicated to directly probe and visualize the electron recollision process [12,15–18].

Since introduced by Bohm [19], Bohmian mechanics has been applied, as an alternative and complementary quantum approach, to the study of a broad range of problems. One approach to Bohmian mechanics is the hydrodynamics formulation of quantum mechanics, in which the probability amplitude and the phase of the wave function are transported along the quantum trajectories, and observables may be computed directly in terms of this information. In the de Broglie–Bohm framework, on the other hand, the individual tracer particles are evolved along quantum trajectories with the velocities generated by the time-dependent wave function field. The patterns developed by these quantum trajectories as they emerge from an ensemble of initial points exactly define the history of the system as it evolves from the initial to final state. This allows one to employ the de Broglie–Bohm framework of Bohmian mechanics (BM) to provide an accurate trajectory-based scheme to interpret the electron wave-packet dynamics [20]. The BM approach has been successfully applied to the model study of problems such as photodissociation [21], tunneling [22], atom diffraction by surface [23], etc., in the past. More recently, it has been also used in the model study of strong field processes such as HHG [24], laser-driven electron dynamics [25–32], etc. Although many of the BM studies of strong field processes so far have adopted either one-dimensional (1D) or soft-potential models, there are also some promising reports that used the de Broglie–Bohm formalism by means of an *ab initio* three-dimensional numerical approach [33].

Although the well-known semiclassical model takes into account the electron-core interaction, due to the lack of phase information, it was proven that this approach may not be suitable to investigate the coherent dynamic processes such as the momentum distribution of the low-energy ATI [15]. An ensemble of individual Bohmian trajectories, within the de Broglie–Bohm framework, on the other hand, contains

—————
[*]jooya@ku.edu
[†]sichu@ku.edu

all the information embedded in the time-dependent wave function. This accurate numerical scheme, therefore, allows tracing the small percentage of the ionized wave packets involved in the rescattering process to reveal the quantum-electron-dynamical origin of the major features appearing in ATI spectra. This method would be a promising candidate to serve as the electron-dynamical analysis tool, in order to provide an intuitive perspective to explain the experimental and numerical observations.

We have recently employed Bohmian mechanics to demonstrate the effect of laser pulse shape on the characteristic properties of high-order-harmonic generation [7] and the subcycle ionization dynamics [34]. In Ref. [34] we showed that, within each optical cycle of the external laser field, some portion of the ionized wave packets, represented by various groups of Bohmian trajectories, return to the parent ion when the laser field changes sign. Since the returning trajectories travel different distances before they change direction and return to the core, each of them would have different return energies. This causes transitions to excited bound and continuum states over time. Therefore, when the next ionization is about to happen (during the subsequent optical cycle), these oscillations of the electron density give rise to multiple wave packets, instead of just one. This effect becomes more and more influential for longer pulse durations (laser field with a higher number of optical cycles). Similar reasoning can be utilized to interpret the HHG and ATI results by evaluating the harmonic emission and energy content of various groups of Bohmian trajectories, which in turn represent the dynamics of different wave packets detached from the parent ion, traveling under the external laser field.

It has been reported [3,12] that the shape and spacing of the photoelectron interference structures in ATI spectra correspond to the specific number of times the electron reencounters its parent ion before scattering away. Our Bohmian calculations indicate that, driven by a 1600-nm laser field, a hydrogenic returning electron wave packet passes the parent ion only if the peak intensity of the laser is as high as 2×10^{14} W/cm^2. Furthermore, we found that the electrons cannot pass the parent ion if the higher-frequency lasers (e.g., 800 nm) are used, even with the intensity of 2×10^{14} W/cm^2. Consequently, the presence of the low-energy photoelectron interference structures for the wavelengths above 800 nm does not necessarily require the multiple electron recollision with its parent ion to happen. This, at the same time, implies that observation of such common structures in ATI spectra is not sufficiently enough to be taken as evidence for the existence of multiple electron revisits.

II. THEORY AND NUMERICAL PROCEDURES

In this paper, we present our results from a fully *ab initio* three-dimensional and accurate treatment of the Bohmian trajectories to explain the role of multiple recollision of photoelectrons in HHG and ATI processes. The time-dependent generalized pseudospectral (TDGPS) method [35] is used to solve the TDSE in spherical coordinates accurately and efficiently and to obtain the time-dependent wave functions for Bohmian mechanics calculations. This method takes advantage of the generalized pseudospectral (GPS) technique for

nonuniform optimal spatial discretization of the coordinates and the Hamiltonian using only a modest number of grid points. Atomic units (a.u.) are used throughout the paper unless specified otherwise. The time propagation of the wave function under this method is performed by the split operator method in the energy representation [35]

$$\psi(r, t + \Delta t) \cong \exp\left(-i\hat{H}_0 \frac{\Delta t}{2}\right) \exp\left[-i V\left(\boldsymbol{r}, \theta, t + \frac{\Delta t}{2}\right) \Delta t\right]$$
$$\times \exp\left(-i\hat{H}_0 \frac{\Delta t}{2}\right) + O(\Delta t^3). \quad (1)$$

For atoms in linearly polarized laser fields, the angular momentum projection onto the polarization direction of the field (the z axis) is conserved. That means the dependence of the wave function on the angle φ (rotation angle about the z axis) is reduced to the factor $\exp(im\varphi)$, where m is the angular momentum projection. For $m = 0$ the wave function does not depend on φ at all; thus the gradient of the wave function ψ can be calculated with respect to the coordinates r (radial coordinate) and θ (angle between the radius-vector and z axis):

$$\boldsymbol{\nabla}\psi = \boldsymbol{e}_r \frac{\partial \psi}{\partial r} + \boldsymbol{e}_\theta \frac{1}{r} \frac{\partial \psi}{\partial \theta} = \boldsymbol{e}_r \frac{\partial \psi}{\partial r} - \boldsymbol{e}_\theta \frac{\sin \theta}{r} \frac{\partial \psi}{\partial \cos \theta}. \quad (2)$$

$\boldsymbol{e}_r$ and $\boldsymbol{e}_\theta$ are the unit vectors of the spherical coordinate system. The equation for the Bohmian trajectories reads as

$$\frac{d\boldsymbol{r}}{dt} = \text{Im} \frac{\boldsymbol{\nabla}\psi}{\psi}. \quad (3)$$

Since the velocity $\frac{d\boldsymbol{r}}{dt}$ has the following expansion in the spherical coordinate system,

$$\frac{d\boldsymbol{r}}{dt} = \boldsymbol{e}_r \frac{dr}{dt} + \boldsymbol{e}_\theta r \frac{d\theta}{dt} + \boldsymbol{e}_\varphi r \sin \theta \frac{d\varphi}{dt}, \quad (4)$$

the vector equation (3) is equivalent to a set of three 1D equations:

$$\frac{dr}{dt} = \text{Im}\left(\frac{1}{\psi} \frac{\partial \psi}{\partial r}\right), \quad (5)$$

$$\frac{d\theta}{dt} = -\frac{\sin \theta}{r^2} \text{Im}\left(\frac{1}{\psi} \frac{\partial \psi}{\partial \cos \theta}\right), \quad (6)$$

$$\frac{d\varphi}{dt} = 0. \quad (7)$$

Obviously, the angle φ does not change, and the trajectory lies in the plane defined by the initial (at $t = t_0$) radius-vector and the z axis. One has to solve the Cauchy problem for the set of two equations (5) and (6). In the generalized pseudospectral (GPS) discretization, we use the Gauss-Lobatto scheme for the variable r (with the appropriate mapping transformation) and the Gauss scheme for the variable $\cos \theta$. The expressions for the first derivatives with respect to r and θ appear in detail in our previous works [7,34]. This set of coupled ordinary differential equations is solved numerically with the help of the fourth-order Runge-Kutta (RK4) method, yielding the electron quantum trajectories.

To obtain the ATI spectra, within the Kramers-Henneberger (KH) frame, we start from the expression for the differential ionization probability corresponding to ejection of the electron with the energy E_f within the unit energy interval and unit

solid angle under the specified direction:

$$\frac{\partial^2 P}{\partial E_f \partial \Omega} = \sqrt{2E_f}|T_{fi}|^2, \tag{8}$$

where Ω denotes the solid angle. For the transition matrix element T_{fi} we use the expression suggested in Ref. [9].

$$T_{fi} = -i \int_0^{t_f} dt \exp\left(iE_f t + \frac{i}{2}\int_0^t \dot{\boldsymbol{b}}^2 d\tau\right) \int d^3 r \, \psi_f^*(\boldsymbol{r} - \boldsymbol{b})$$
$$\times [U(\boldsymbol{r}) - U(\boldsymbol{r} - \boldsymbol{b})] \exp[-i(\dot{\boldsymbol{b}} \cdot \boldsymbol{r})]\psi(\boldsymbol{r},t). \tag{9}$$

Here, the time-dependent quantity $\boldsymbol{b}$ has the meaning of the displacement of the "classical" electron under the influence of the laser field only; a dot above $\boldsymbol{b}$ denotes the first derivative with respect to time. The potential $U(\boldsymbol{r})$ represents the interaction with the atomic core; the term $U(\boldsymbol{r}) - U(\boldsymbol{r} - \boldsymbol{b})$ decreases at least as $1/r^2$ at large $\boldsymbol{r}$; therefore, the spatial integration in Eq. (9) emphasizes the core region of the wave packet. The wave function $\psi(\boldsymbol{r},t)$ satisfies the time-dependent Schrödinger equation:

$$i\frac{\partial}{\partial t}\psi(\boldsymbol{r},t) = \left[-\frac{1}{2}\nabla^2 - (\ddot{\boldsymbol{b}} \cdot \boldsymbol{r}) + U(\boldsymbol{r})\right]\psi(\boldsymbol{r},t). \tag{10}$$

It takes into account the interactions with both the atomic core and laser field (the latter interaction is described in the length gauge; $\ddot{\boldsymbol{b}}$ is the classical acceleration). Before the laser pulse, this function coincides with the initial bound state of the electron.

The final state of the electron $\psi_f(\boldsymbol{r})$ describes motion in the atomic field only. As discussed in the scattering theory [36], the correct final states for calculation of the angular distributions are the functions $\bar{\psi}_k(\boldsymbol{r})$ which have plane waves and incoming spherical waves asymptotically at large distances. They satisfy the following orthogonality and normalization condition:

$$\langle \bar{\psi}_{k'}(\boldsymbol{r})|\bar{\psi}_k(\boldsymbol{r})\rangle = \delta^{(3)}(\boldsymbol{k} - \boldsymbol{k}'). \tag{11}$$

The final continuum states $\bar{\psi}_k(\boldsymbol{r})$ in the Coulomb field are known in a closed form,

$$\bar{\psi}_k(\boldsymbol{r}) = \frac{1}{2\pi}\sqrt{\frac{v}{\exp(2\pi v) - 1}}\exp[i(\boldsymbol{k} \cdot \boldsymbol{r})]$$
$$\times M\{iv,1,-i[kr + (\boldsymbol{k} \cdot \boldsymbol{r})]\}, \tag{12}$$

where $M(a,c,x)$ is the confluent hypergeometric function. v is the Coulomb parameter; $v = -Z_c/k$.

All the calculations for the current study are performed for a hydrogen atom subject to linearly polarized midinfrared laser fields. The laser pulse has a sine-squared envelope, $F(t) = F_0\sin^2(\frac{\pi t}{T})\sin(\omega t)$, where F_0 is the peak field amplitude, ω is the carrier frequency, and T is the pulse duration. First, we study the mechanism of multiple recollision when $\lambda = 1600$ nm (corresponding to $\omega = 0.0285$ a.u.) with two peak intensities, 5×10^{13} and 2×10^{14} W/cm². In our investigations, we have considered several wavelengths, finding that for $\lambda = 1600$ nm the multiple recollision effect is more pronounced and the results are more striking, which are the ones here reported. To be able to better identify and understand the role of multiple recollision in HHG and ATI processes, we limit our results for the case of four optical cycle laser fields.

The expectation value of the dipole acceleration is obtained from the time-dependent wave function:

$$d_A(t) = \langle \psi(\boldsymbol{r},t)| - \frac{z}{r^3} + F(t)|\psi(\boldsymbol{r},t)\rangle. \tag{13}$$

The corresponding HHG power spectrum from a hydrogen atom exposed to the laser field is obtained, on the single-atom level, by the Fourier transformation of time-dependent dipole acceleration as follows [37]:

$$P_A(\omega) = \left|\frac{1}{t_f - t_i}\frac{1}{\omega^2}\int_{t_i}^{t_f} d_A(t)e^{-i\omega t}\right|^2. \tag{14}$$

III. RESULTS AND DISCUSSION

In Fig. 1, we use Bohmian trajectories to provide a complete illustrative picture of the hydrogenic photoelectron dynamics under four optical cycle 1600-nm sine-squared laser pulses with two different intensities of 5×10^{13} and 2×10^{14} W/cm²(presented in the top boxes in Fig. 1). The red and green trajectories presented in Fig. 1 are obtained from two separate sets of Bohmian calculations. For the green trajectories we set the initial condition in the z direction to be $+1 \leqslant z_0 \leqslant +20$, and for the red trajectories we use $-1 \leqslant z_0 \leqslant -20$. For both cases, $x_0 = 1$ (all in atomic units). Although the proposed method is robust and is not sensitive to the selected initial conditions, we found that this set best represents the dynamics of an electron under the given laser fields. The right panels, in Fig. 1, schematically display the characteristic trajectories for each case. The first immediate observation is the presence of multiple revisits under the stronger laser pulse, Fig. 1(b); this feature is obviously absent in the case of a weaker laser field, Fig. 1(a). Under the 5×10^{13} W/cm² laser pulse, Fig. 1(a), the emitted electron traveling toward the positive or negative z direction stays on one side of the parent ion. In this case the electron is pulled back when the laser field changes sign, and eventually scatters away from the same side of the atom (after some oscillations under the influence of the laser field). At the higher intensity, 2×10^{14} W/cm² [Fig. 1(b)], however, the returning trajectories are strongly pulled over the parent ion and therefore penetrate into the opposite z direction. As can be seen in Fig. 1(b), this effect is influential only around and after the laser peak, when the driving external field is strong enough. In both cases, all the sequential returning groups of Bohmian electron trajectories are numerically labeled for further analysis. In particular, it is worth mentioning that in Fig. 1(b) the trajectories exhibiting two rescattering events are marked "4" and "6." The second return of the green trajectories is labeled "4," and the one corresponding to the red trajectories is labeled "6." These groups of Bohmian trajectories represent the electron wave packets that return to the core from the opposite direction of their initial detachment. In the remaining part of this article we will investigate the contribution of each of these ensemble trajectories to harmonic generation. The big circular arrows in Fig. 1(a) schematically display how the ejected electrons are distributed in momentum content.

The tails of these arrows correspond to the higher-momentum traveling electrons. These are electrons that are expected to have higher velocities, due to the fact that they are represented by trajectories with higher slopes,
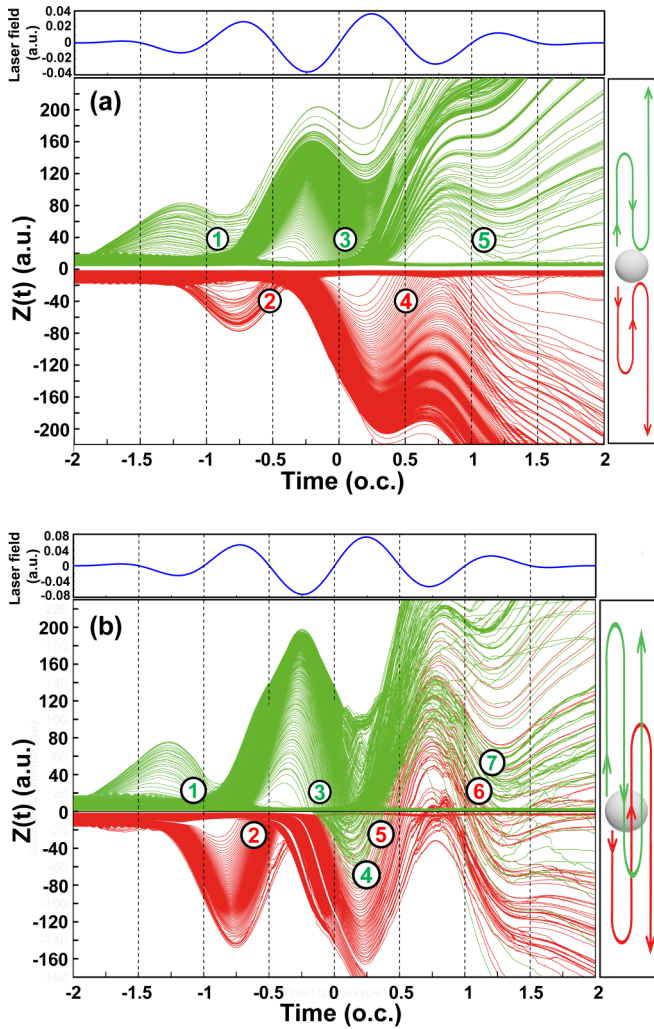
FIG. 1. Bohmian trajectories illustrating the dynamics of hydrogenic electron wave packets initially traveling toward the negative (red) and positive (green) z directions; time is measured in optical cycles (o.c.). These results are obtained by solving the coupled system of Eqs. (5) and (6). The driving laser field is a four optical cycle 1600-nm sine-squared laser pulse with (a) 5×10^{13} W/cm^2 and (b) 2×10^{14} W/cm^2 peak intensity. In each case, the sequential returning groups of Bohmian electron trajectories are numerically labeled for further analysis. The top panels present the driving laser fields and the right panels schematically display the characteristic trajectories for each case. The characteristic feature under study is double revisits, which are only present when the electron is traveling under high-intensity midinfrared laser field (b). The big circular arrows in (a) schematically display how the ejected electrons are distributed in momentum content. This roughly represented feature is valid for other laser field cases in this study.

dZ/dt, in the presented plots in Fig. 1. Being valid for the other laser field cases, this roughly represented feature will help us to better interpret some of the structural aspects of the ATI spectra. Time evolution of individual trajectories will be closely analyzed to address some of the main features of the photoelectron angular distributions for atoms subject to intense midinfrared laser fields.

The results presented in Fig. 2 are the HHG time-frequency profiles obtained by the wavelet transformation of the dipole acceleration [Eq. (13)] of the hydrogen atom driven by the two given laser fields. The HHG wavelet time-frequency profile is considered as unambiguous evidence of the existence of the bremsstrahlung radiation which is emitted by the recollision of the electron wave packet with the parent ionic core. In each presented profile, the deeper blue color indicates that a relatively larger number of electron trajectories contribute to generation of those particular harmonics. The presented wavelet profiles, together with the information obtained from the Bohmian mechanics, Fig. 1, provide a comprehensive and intuitive picture of the HHG process and the role of multiple rescattering events. For each case in Figs. 2(a) and 2(b), the dominant groups of the trajectories in generation of the emission peaks in the wavelet profiles are indicated by the same numbers as in Fig. 1. This correlation is made by close comparison between the harmonic peaks' emission times in Fig. 2 and the return time period of each group of the Bohmian trajectories in Fig. 1. The first noticeable difference between the two wavelet profiles is the existence of three main peaks in Fig. 2(a), contrary to five peaks in Fig. 2(b). This difference can be simply explained by observing the strongly driven or returning trajectories labeled "1" and "2" in Fig. 1(b), contrary to similarly labeled groups of slightly driven trajectories under weaker laser field in Fig. 1(a). In other words, the initially detached traveling trajectories under 5×10^{13} W/cm^2, labeled "1" and "2" in Fig. 1(a), do not gain enough energy under the external field to be able to have a noticeable contribution in the harmonics generation upon the return. In addition, one of the most prominent features in Fig. 2(b) is the appearance of two subpeaks (indicated by arrows and labeled "4" and "6") at the second half of the time propagation of the electron under the driving high-intensity laser field. These harmonic emissions are considered to be caused by the recombination of the second revisiting electron wave packets with the parent ions. The trajectories representing these electrons have labels "4" and "6" in Fig. 1(b).

The differential ionization probabilities, obtained from Eq. (8), at the end of each of these laser pulses are presented in Fig. 3. The polar surface plots of the differential ionization probabilities are shown in Figs. 3(a) and 3(c). The radial distance on these plots represents the energy and the angle points to the direction where the electron is ejected (with respect to the polarization of the laser field). The density (color) shows the differential ionization probability (in logarithmic scale). There are two immediate observations: (i) Regarding the angular distributions, one can see that in Fig. 3(a) the electrons (under the 5×10^{13} W/cm^2 laser field) are mostly ejected in the field direction; however, noticeable side lobes are present in Fig. 3(c) (the 2×10^{14} W/cm^2 laser field), which indicates the prominent distribution of the electron wave packets toward the x direction. (ii) In Fig. 3(c), close comparison of the positive and negative momentum distributions shows fine structure of each ATI peak in the right half-space. This also can be seen in panels (b) and (d), which compare the corresponding energy spectrum for the electrons emitted in the polarization direction of these laser fields, respectively. In each case, the dashed red line shows the spectrum for the electrons ionizing toward the negative z direction, and the solid blue line presents the electrons traveling toward the positive z direction. In Fig. 3(b), one can see a similar pattern (position and the intensity of the
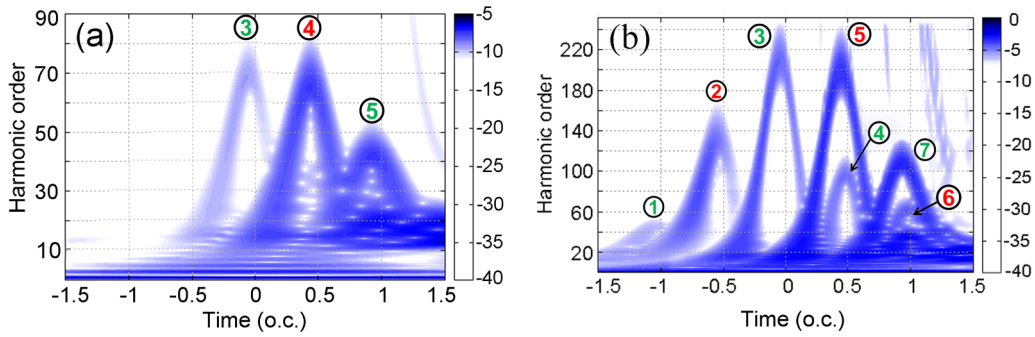
FIG. 2. HHG time-frequency profile obtained by the wavelet transformation of the dipole acceleration [Eq. (13)] of the hydrogen atom driven by a four optical cycle 1600-nm sine-squared laser pulse with the peak intensities of (a) 5×10^{13} W/cm^2 and (b) 2×10^{14} W/cm^2. Time is measured in optical cycles (o.c.), and the color scale is logarithmic. The numerical labels are the same as in Fig. 1. These numbers indicate which groups of the Bohmian trajectories have dominant contributions to each main harmonic emission peak. The subpeaks indicated by the arrows in (b) are due to the recombination of the second-revisiting electrons marked "4" and "6" in Fig. 1(b).

peaks) for both presented plots. Both of these energy spectra exhibit the well-known ATI structure with the peaks separated by a photon energy ω. The similarity between these two plots demonstrates the relatively equal contribution of the electron wave packets traveling toward the negative and positive z

directions. The energy spectra under the 2×10^{14} W/cm^2 laser field, however, illustrate clearly different patterns for the opposite-direction traveling electron wave packets. Along with the comprehensive picture provided by the Bohmian trajectories, this can serve as evidence for the existence of
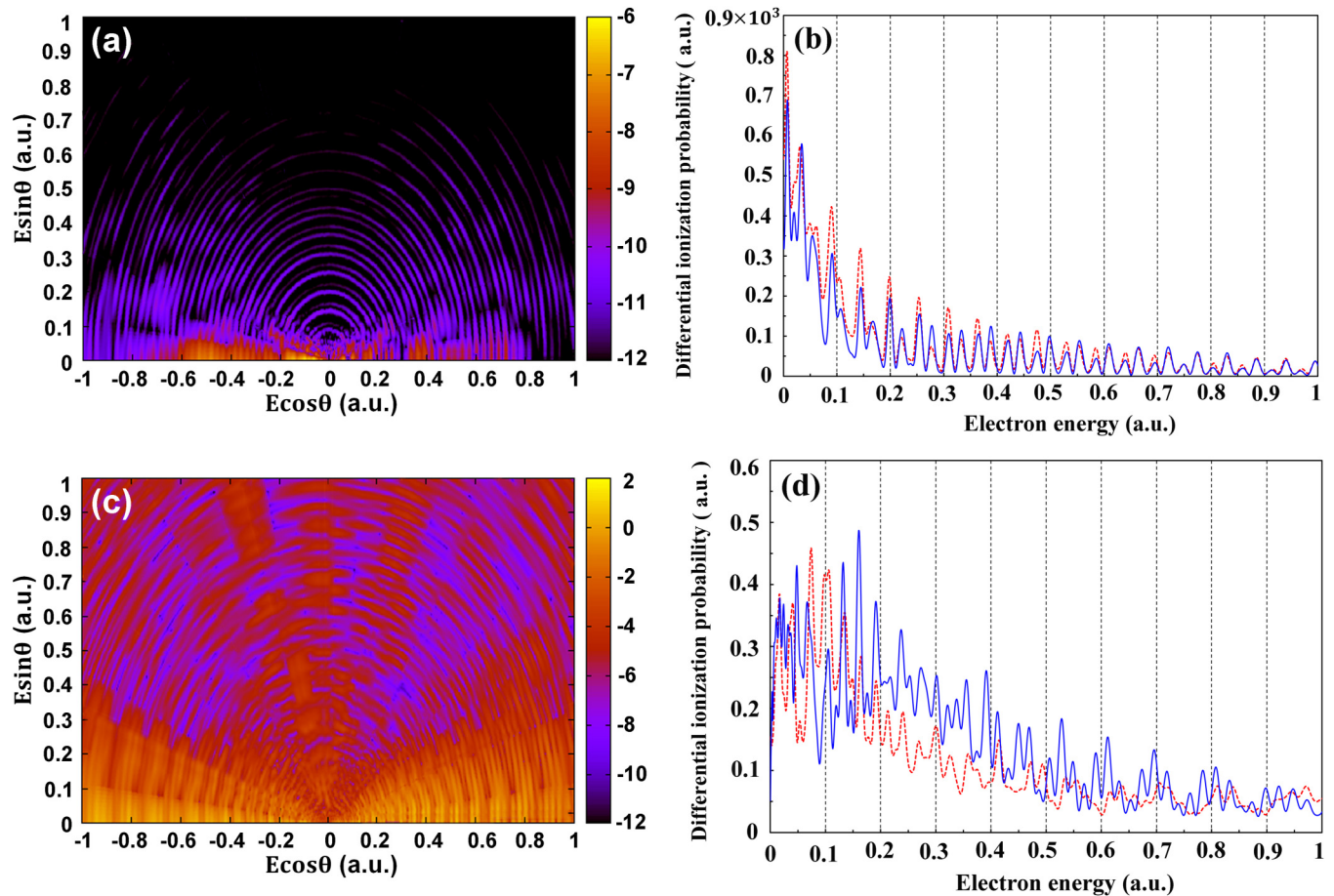
FIG. 3. (a,c) Energy-angle polar surface plots of differential ionization probability. The color scale represents the logarithm of the quantity defined by Eq. (8). θ is the ejection angle with respect to the polarization of the laser field. The carrier wavelength of the laser pulse is 1600 nm and the duration is four optical cycles. The peak intensity is 5×10^{13} W/cm^2 for (a), and 2×10^{14} W/cm^2 for (c). For each case, the energy spectrum for the electrons emitted in the polarization direction of the laser field is given in panels (b) and (d), respectively. The dashed red line shows the spectrum for the electrons traveling toward the negative z direction, and the solid blue line presents the electrons traveling toward the positive z direction.
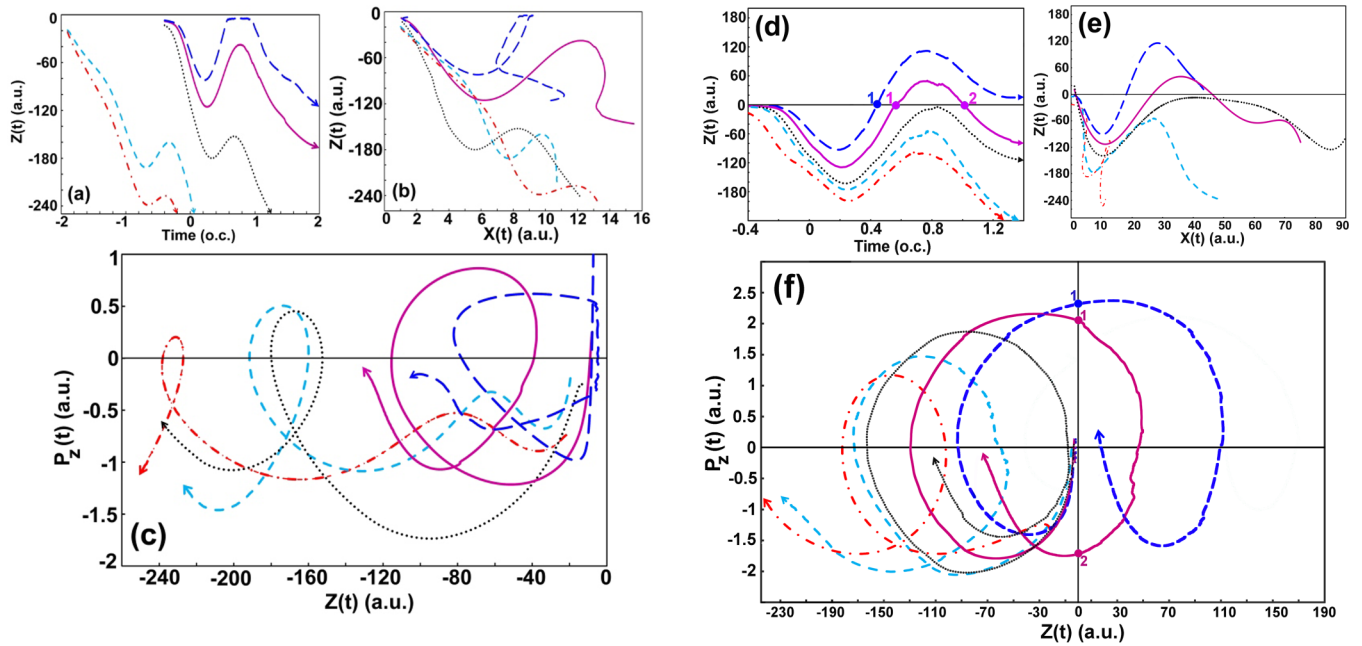
FIG. 4. Selected Bohmian trajectories, representing various groups of trajectories from Fig. 1. (a–c) illustrate the dynamics of the electron wave packets which are initiated, and then travel and scatter away from the negative z direction, under the influence of a 1600-nm four optical cycle $\sin^2$ laser pulse with the peak intensity of 5×10^{13} W/cm^2; time is measured in optical cycles (o.c.). (a) The time evolution of the electron position in the z direction. (b) The same trajectories in the xz plane. (c) The phase diagram showing how the momentum changes with the distance in the field direction. (d–f) present similar results when the laser peak intensity is 2×10^{14} W/cm^2. The revisits of the electron are labeled "1" and "2" in panels (d) and (f). These results are obtained by solving the coupled system of Eqs. (5) and (6).

multiple (in this case, two) revisits of the electron. Figure 1(b) shows that under the incident laser field, big portions of the electron wave packets that initially detached toward the negative z direction [represented by the red trajectories in Fig. 1(b)] end up scattering away from the positive z direction. A similar contribution (in energy) of these electron trajectories (in red) with the ones that are initiated and scattered away from the positive z direction (in green) should be held responsible for the appearance of the fine structure in the right half-space of Fig. 3(c), which is reflected in the corresponding energy spectrum in Fig. 3(d) (blue solid line) as well.

In Fig. 4, we study the time evolution of some selected individual Bohmian trajectories, for the case of the laser fields with the peak intensities of 5×10^{13} W/cm^2 [Figs. 4(a)–4(c)] and 2×10^{14} W/cm^2 [Figs. 4(d)–4(f)]. In resemblance to Fig. (1), in each case, the displacement of the electron particle tracer in the z direction is given in panels (a) and (d). The number of revisits of the electron under the stronger (2×10^{14} W/cm^2) laser field is also given in Figs. 4(d) and 4(f). Comparison of the trajectories in the xz plane from panels (b) and (e) provides the explanation for the first observation, (i), we made around Fig. 3. As one can see in Fig. 4(b), under the weaker laser field, the detached electron wave packets are mainly distributed in the direction of the laser field and have only small spreading in the x direction (maximum traveling distance in this direction is less than 16 a.u.). As illustrated in Fig. 4(e), however, the detached electron may travel up to about 90 a.u. perpendicular to the field direction with the peak intensity of 2×10^{14} W/cm^2. This observation explains the presence of noticeable side lobes in the ATI spectrum in Fig. 3(c). This can also serve as additional evidence for

multiple transit of the electron over its parent ion subject to a strong midinfrared laser field. Panels (c) and (f) show how the momentum is changing with respect to the distance in the direction of the driving laser field for the selected individual Bohmian trajectories. The prominent observation here is that the trajectories traveling close to each other in space would be carrying similar energy content at their final state. This observation, therefore, supports our previous statement regarding the presence of the fine structure in the ATI spectrum in Fig. 3(c), and the corresponding energy spectrum in Fig. 3(d) (blue solid line).

IV. SUMMARY

In summary, we used fully *ab initio* three-dimensional and accurate Bohmian mechanics results to illustrate the role of electron multiple recollisions in some of the main features observed in HHG and ATI spectra. Contrary to semiclassical calculations, Bohmian trajectories contain all the information embedded in the time-dependent wave function. This makes the method suitable to investigate the coherent dynamic processes for which the phase information is crucial. In this study, the appearance of the subpeaks in the high-harmonic-generation time-frequency profiles and the asymmetric fine structures in the above-threshold ionization spectrum were analyzed by the comprehensive and intuitive picture provided by Bohmian mechanics. The commonly accepted evidence for multiple revisits of an electron in the ATI spectra was reevaluated and a clear, distinct pattern in the HHG spectra which demonstrates the occurrence of multiple revisits in wavelet time-frequency profiles is

explained by the comprehensive picture provided by Bohmian mechanics.

ACKNOWLEDGMENTS

[1] P. B. Corkum, Phys. Rev. Lett. **71**, 1994 (1993).

[2] M. Lewenstein, Ph. Balcou, M. Yu. Ivanov, A. L'Huillier, and P. B. Corkum, Phys. Rev. A **49**, 2117 (1994).

[3] U. Mohideen, M. H. Sher, H. W. K. Tom, G. D. Aumiller, O. R. Wood II, R. R. Freeman, J. Boker, and P. H. Bucksbaum, Phys. Rev. Lett. **71**, 509 (1993).

[4] X. M. Tong, P. Ranitovic, D. D. Hickstein, M. M. Murnane, H. C. Kapteyn, and N. Toshima, Phys. Rev. A **88**, 013410 (2013).

[5] T. Tate, T. Auguste, H. G. Muller, P. Salieres, P. Agostini, and L. F. DiMauro, Phys. Rev. Lett. **98**, 013901 (2007).

[6] Y. Mairesse, A. de Bohan, L. J. Frasinski, H. Merdji, L. C. Dinu, P. Monchicourt, P. Breger, M. Kovačev, T. Auguste, B. Carré, H. G. Muller, P. Agostini, and P. Salières, Phys. Rev. Lett. **93**, 163901 (2004).

[7] H. Z. Jooya, D. A. Telnov, P. C. Li, and S. I. Chu, J. Phys. B: At., Mol. Opt. Phys. **48**, 195401 (2015).

[8] D. A. Telnov and S. I. Chu, Phys. Rev. A **83**, 063406 (2011).

[9] D. A. Telnov and S. I. Chu, Phys. Rev. A **79**, 043421 (2009).

[10] C. Liu, and K. Z. Hatsagortsyan, Phys. Rev. Lett. **105**, 113003 (2010).

[11] T. M. Yan, S. V. Popruzhenko, M. J. J. Vrakking, and D. Bauer, Phys. Rev. Lett. **105**, 253002 (2010).

[12] D. D. Hickstein, P. Ranitovic, S. Witte, X.-M. Tong, Y. Huismans, P. Arpin, X. Zhou, K. E. Keister, C. W. Hogle, B. Zhang, C. Ding, P. Johnsson, N. Toshima, M. J. J. Vrakking, M. M. Murnane, and H. C. Kapteyn, Phys. Rev. Lett. **109**, 073004 (2012).

[13] A. Gazibegovic-Busuladzic, D. B. Milosevic, W. Becker, B. Bergues, H. Hultgren, and I. Yu. Kiyan, Phys. Rev. Lett. **104**, 103004 (2010).

[14] M. Li, X. Sun, X. Xie, Y. Shao, Y. Deng, C. Wu, Q. Gong, and Y. Liu, Sci. Rep. **5**, 8519 (2015).

[15] X. M. Tong, S. Watahiki, K. Hino, and N. Toshima, Phys. Rev. Lett. **99**, 093001 (2007).

[16] O. Smirnova, S. Patchkovskii, and M. Spanner, Phys. Rev. Lett. **98**, 123001 (2007).

[17] M. H. Xu, L. Y. Peng, Z. Zhang, Q. Gong, X. M. Tong, E. A. Pronin, and A. F. Starace, Phys. Rev. Lett. **107**, 183001 (2011).

[18] A. Kastner, U. Saalmann, and J. M. Rost, Phys. Rev. Lett. **108**, 033201 (2012).

[19] D. Bohm, Phys. Rev. **85**, 166 (1952).

[20] R. E. Wyatt, Quantum Dynamics with Trajectories, *Interdisciplinary Applied Mathematics* Vol. 28 (Springer, Berlin, 2000).

[21] F. S. Mayor, A. Askar, and H. Rabitz, J. Chem. Phys. **111**, 2423 (1999).

[22] C. L. Lopreore and R. E. Wyatt, Phys. Rev. Lett. **82**, 5190 (1999).

[23] R. Guantes, A. Sanz, J. Margalef-Roig, and S. Miret-Artes, Surf. Sci. Rep. **53**, 199 (2004).

[24] J. Wu, B. B. Augstein, and C. F. d. M. Faria, Phys. Rev. A **88**, 023415 (2013).

[25] P. Botheron and B. Pons, Phys. Rev. A **82**, 021404(R) (2010).

[26] R. Sawada, T. Sato, and K. L. Ishikawa, Phys. Rev. A **90**, 023404 (2014).

[27] J. Wu, B. B. Augstein, and C. F. de Morisson Faria, Phys. Rev. A **88**, 063416 (2013).

[28] S. S. Wei, S. Y. Li, F. M. Guo, Y. J. Yang, and B. Wang, Phys. Rev. A **87**, 063418 (2013).

[29] J. Stenson and A. Stetz, Eur. J. Phys. **34**, 1199 (2013).

[30] N. Takemoto and A. Becker, J. Chem. Phys. **134**, 074309 (2011).

[31] S. Dey and A. Fring, Phys. Rev. A **88**, 022116 (2013).

[32] Y. Song, F. M. Guo, S. Y. Li, J. G. Chen, S. L. Zeng, and Y. J. Yang, Phys. Rev. A **86**, 033424 (2012).

[33] A. Picon, A. Benseny, J. Mompart, J. R. Vazquez de Aldana, L. Plaja, G. F. Calvo, and L. Roso, New. J. Phys. **12**, 083053 (2010).

[34] H. Z. Jooya, D. A. Telnov, P. C. Li, and S. I. Chu, Phys. Rev. A **91**, 063412 (2015).

[35] X. M. Tong, and S. I. Chu, Chem. Phys. **217**, 119 (1997).

[36] R. G. Newton, *Scattering Theory of Waves and Particles* (McGraw-Hill, New York, 1966).

[37] H. Z. Jooya, P. C. Li, S. L. Liao, and S. I. Chu, Phys. Lett. A **380**, 316 (2016).